Modeling universal dynamics of cell spreading on elastic substrates

Houfu Fan & Shaofan Li

Biomechanics and Modeling in Mechanobiology

ISSN 1617-7959

Biomech Model Mechanobiol
DOI 10.1007/s10237-015-0673-1

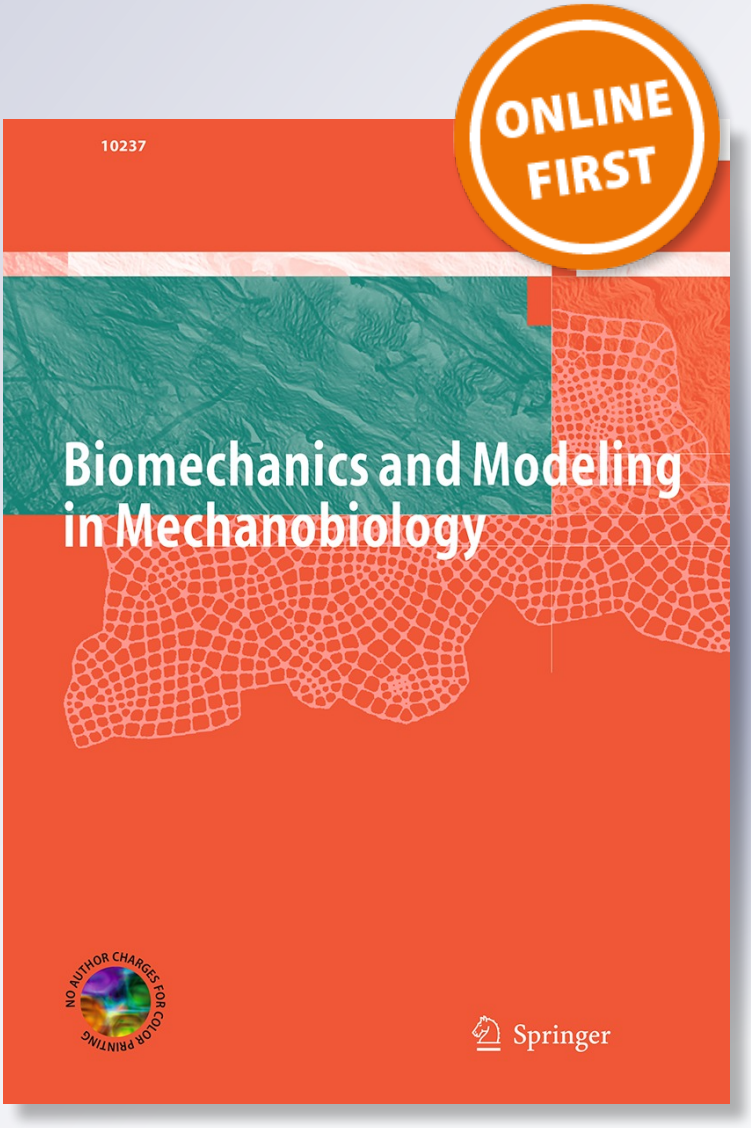

Springer

Biomech Model Mechanobiol
DOI 10.1007/s10237-015-0673-1

ORIGINAL PAPER

Modeling universal dynamics of cell spreading on elastic substrates

Houfu Fan[1] · **Shaofan Li**[1]

Received: 16 December 2014 / Accepted: 31 March 2015

Abstract A three-dimensional (3D) multiscale moving contact line model is combined with a soft matter cell model to study the universal dynamics of cell spreading over elastic substrates. We have studied both the early stage and the late stage cell spreading by taking into account the actin tension effect. In this work, the cell is modeled as an active nematic droplet, and the substrate is modeled as a St. Venant Kirchhoff elastic medium. A complete 3D simulation of cell spreading has been carried out. The simulation results show that the spreading area versus spreading time at different stages obeys specific power laws, which is in good agreement with experimental data and theoretical prediction reported in the literature. Moreover, the simulation results show that the substrate elasticity may affect force dipole distribution inside the cell. The advantage of this approach is that it combines the hydrodynamics of actin retrograde flow with moving contact line model so that it can naturally include actin tension effect resulting from actin polymerization and actomyosin contraction, and thus it might be capable of simulating complex cellular scale phenomenon, such as cell spreading or even crawling.

Keywords Adhesive contact · Cell spreading · Moving contact line · Cell crawling · Soft matter

1 Introduction

Cell spreading is a fundamental biological process that plays a vital role in many cellular processes such as cell crawling, proliferation, wound healing, tumor metastasis, drug delivering and artificial culture design for tissue engineering. Cell spreading process can be categorized into two distinct stages (Cuvelier et al. 2007; Dobereiner et al. 2004; McGrath 2007): the early stage and the late stage. In the early stage, the cell initially contacts with the extracellular matrix (ECM) and senses the ligands on the substrate. Generally speaking, the early stage cell spreading is a passive process, in which the cell remains in suspension and presents a roughly spherical morphology. During this stage, the cell deformation is purely mechanical, which disrupts the cortical cytoskeleton. Due to the lack of focal contacts, the interaction of the cell and the ECM is very weak. Once the contact area reaches a threshold along with the disruption of the cortical cytoskeleton, the cell spreading will enter the late stage, in which the cell is activated by the rapid increase in certain proteins resulting from the ligand–receptor adhesion. These proteins will cause steady-state polymerization of the cortical actin in the cytoskeletal network, leading to an increase in the protrusive forces and ligand–receptor adhesion sites. These protrusive forces will facilitate the motion or extension of the lamellipodia and filopodia, causing the cell spreading area continuously increase. Aside from actin polymerization, another feature of the late stage cell spreading is contractility of the cell cytoskeleton, accomplished by the actomyosin-based stress fibers linked to focal adhesions. The contractile forces serve as the dynamism to detach the cell from the substrate or compress and reconstruct the corresponding extracellular matrix. It is worth noting that the late stage of cell spreading is governed by both the actin polymerization and myosin dependent contraction. It is the combination of the two that decides the cell margin will extend or contract (Cai et al. 2006; Wakatsuki 2003). Despite its complexity and diversity, it is believed that there is a universal dynamics in the spreading process of a living cell.

✉ Shaofan Li
shaofan@berkeley.edu

[1] Department of Civil and Environmental Engineering, University of California, Berkeley, CA 94720, USA

Published online: 08 April 2015

Recently there have been a lot of efforts on the modeling of cellular behaviors, like adhesion, spreading or crawling. Zemel et al. (2010) investigated the shape, symmetry and polarization of stress fibers during the process of cell spreading. It was demonstrated, by combining a simple elastic model and experiments on stem cells, that the alignment of actomyosin forces increases monotonically with matrix rigidity when the cell spreading is sufficiently asymmetric, in sharp contrast to the previous understanding that the alignment is generally non-monotonic. Using a simple mechanical model, together with experimental measurements, Nisenholz et al. (2014) analyzed the temporal force balance between cell and the substrate during cell spreading. It is found that cell area and force increase simultaneously during spreading, but the force presents with a delay relative to increase in cell area, which reflects the strain-stiffening property of the cytoskeleton. By conducting experiments on human endothelial cells, Brill–Karniely et al. (2014) also found that cell area and force increase simultaneously with different rates, which are explained by three complementary mechanisms. Vernerey and Farsad (2014) proposed a mathematical model that couples cell adhesion, contraction and spreading. It is shown that the model is able to capture the dependency of cell spreading and contraction on substrate stiffness and the effect of chemistry, which to some extent suggests the importance of mechanics in the process of cell spreading. Bischofs et al. (2009) introduced a mechanical model that can predicts cellular force distributions during cell adhering (Bischofs et al. 2009). Albert and Schwarz (2014) proposed a three-dimensional (3D) Potts model to capture dynamic and steady states of cell shape and forces without any prior knowledge on the cell spreading process on a given micro-patterned substrate (Albert and Schwarz 2014). Giomi and DeSimone (2014) employed a model of active nematic droplets that is embedded in an isotropic Netwonian fluid, and they successfully captured the spontaneous division and motility, a reminiscent of the behaviors from a typical living cell (Giomi and DeSimone 2014). These modeling efforts on cellular motions are successful in their respective fields or perspectives. Nevertheless, investigations on the spreading of living cells are mainly studied through experiments (Dubin-Thaler et al. 2008; Fardin et al. 2010; Li et al. 2014; Vianay et al. 2010), accompanied by some intuitive or phenomenologically explanations. To the best of the authors' knowledge, there are very few direct 3D modelings and simulations by computational mechanics/soft matter physics on cellular motions that can successfully capture the cell spreading process, if there is any at all.

Contact angle is a crucial physical concept in explaining a variety of phenomena occurred at liquid–solid interfaces, such as durotaxis of cells, capillary action and floating of a water droplet on a lotus leaf and etc. The dynamic wetting process of a water droplet upon a solid substrate can be modeled by using the moving contact line (MCL) hydrodynamics theory (Blake 2006; Minaki and Li 2014). However, this continuum approach faces great challenges, because of its assumption on no-slip condition, which states that no relative motion is allowed at the liquid–solid interface (definition of the MCL), leading to an infinite shear stress value on the solid substrate at the MCL (Blake 2006; Minaki and Li 2014; Shikhmurzaev 2006). In this paper, a multiscale moving contact line (MMCL) theory is developed, and it can be employed to simulate droplets spreading on various elastic substrates. The MMCL uses a coarse-grained contact model (CGCM) (Sauer and Li 2007a, b, 2008) to treat the adhesive contact interaction between liquid phase and solid phase, so that the water droplet is levitated by the intermolecular forces between the liquid and the corresponding substrate, and hence the singularity problem of the conventional MCL is resolved.

Recently, Style et al. (2013) found that water droplets can spread or even move, by simply modulating the stiffness of the underlying substrate (Style et al. 2013). These striking behaviors of water droplets present great similarities to those of living cells. In fact, several researchers have proposed to treat cell spreading process as that of the traditional wetting transition (Douezan et al. 2011; Frisch and Thoumine 2002; Sackmann and Bruinsma 2002). In addition, Gabella et al. (2014) incorporate the contact angle concept into the migration of living cells, by considering the actin tension forces generated through polymerization of the cytoskeleton or actomyosin contraction at the cell leading edge (Gabella et al. 2014).

In this work, we propose to combine the MMCL theory with a soft matter cell model (Zeng and Li 2012), so that we can conduct quantitatively study of cell spreading over elastic substrates. In our simulations, cells are modeled as nematic droplets, which have been used to simulate cellular level behaviors by many researchers (Joanny and Prost 2009; Julicher et al. 2007; Zeng and Li 2012). And without loss of generality, the substrate is modeled as a St. Venant Kirchhoff elastic medium. The main novelty and distinction of the present work are the synergy of the following two aspects: (1) A MMCL theory is developed so that it can simulate dynamic droplet spreading, and (2) the active effect (actin polymerization or actomyosin contraction) is incorporated into the MMCL framework. The combination of the two enables us to model complex active cellular phenomena, such as extensive cell spreading or even crawling (Dubin-Thaler et al. 2008).

The model is implemented in a Lagrange type of Galerkin finite element weak formulations. Early stage cell spreading simulations are first performed. In the early stage spreading, the main driving force comes from the surface energy of the cell membrane and the corresponding substrate adhesion/contact. Then late stage cell spreading simulations with the active effect from actin polymerization or actomyosin

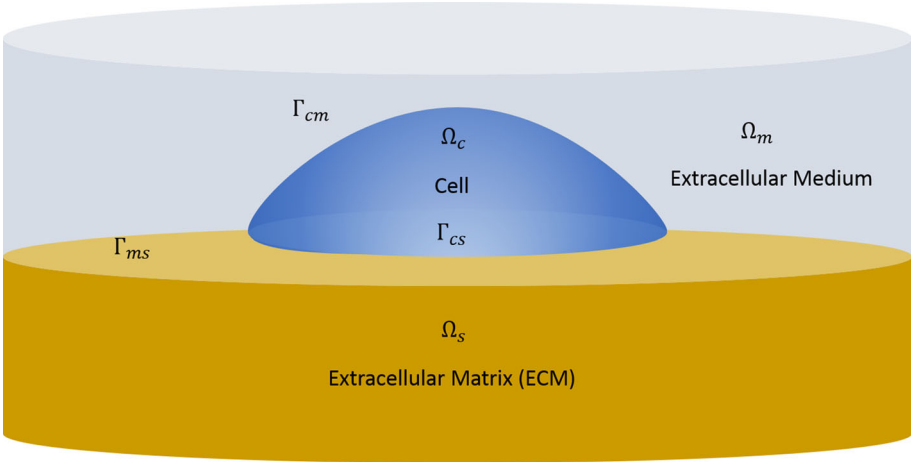

Fig. 1 Schematic illustration of three-phase interacting system

contraction are carried out. Simulations of cells spreading upon substrates with different stiffness are conducted, hoping to shed some light on the mechanotransduction of living cells. The simulation has shown that complete 3D cell spreading modeling can be accomplished by the model proposed. In addition, the numerical data of spreading area verse spreading time at different spreading stages obtained from the simulation results indicates a power law, which is in good agreement with experiments and theoretic prediction in the literature. Moreover, comparison studies of the cell spreading upon substrate with various elasticities revealed the mechanotransduction between cells and their surrounding environment.

The presentation of the paper is organized as follows: In Sect. 2, a general description of the theoretic model is offered, with special attention on the incorporating of the actin polymerization and possible actomyosin effects. In Sect. 3, a few numerical examples are presented. In Sect. 4, we close our presentation by making a few remarks.

2 Simulation model

Before proceeding to any detailed theory, we would like to present the global picture of the model problem. In specific, we are considering the following triple-phase system that consists of a cell Ω_c, an extracellular matrix Ω_s and surrounding extracellular medium Ω_m, as shown in Fig. 1. Throughout this paper, the bulk index $c, sandm$ refers to the cell, the extracellular matrix and the extracellular medium, respectively. The interfaces of the triple-phase system are labeled as $\Gamma_{\rm cs}$, $\Gamma_{\rm ms}$ and $\Gamma_{\rm cm}$. The moving contact line is denoted as $\Gamma_{\rm mcl} = \Gamma_{\rm cs} \cap \Gamma_{\rm ms} \cap \Gamma_{\rm cm}$. The three phases are subjected to the conventional equations of motion in the bulk, a series of surface equations of motion, mutual interaction forces among the three phases and the active effects (actin polymerization or actomyosin contraction) from the cell.

2.1 Incorporating the active effects

In this section, we aim to present a very simple demonstration in explaining the basic idea on how the active effect can be incorporated. Consider the 2D case of a cell placed on an elastic substrate embedded in the ambient space with permissable conditions, as shown in Fig. 2a. Using the MMCL theory, the nodal force on the node at the moving contact line $\Gamma_{\rm mcl}$ can be obtained as (this equation will be provided later in the paper),

$$\begin{aligned}\mathbf{F}_I^s &= -\left(\int_{\Gamma_{\rm cs}} \frac{\partial N_I}{\partial \mathbf{x}} \cdot \gamma_{\rm cs}\mathbf{I}_s^{(cs)}\mathrm{d}s + \int_{\Gamma_{\rm lg}} \frac{\partial N_I}{\partial \mathbf{x}} \cdot \gamma_{\rm cm}\mathbf{I}_s^{(\rm cm)}\mathrm{d}s \right.\\ &\quad \left. + \int_{\Gamma_{\rm gs}} \frac{\partial N_I}{\partial \mathbf{x}} \cdot \gamma_{\rm ms}\mathbf{I}_s^{(\rm ms)}\mathrm{d}s\right)\\ &= -\gamma_{\rm cs}\begin{pmatrix}1\\0\end{pmatrix} - \gamma_{\rm cm}\begin{pmatrix}\cos\theta\\-\sin\theta\end{pmatrix} - \gamma_{\rm ms}\begin{pmatrix}-1\\0\end{pmatrix}\\ &= \begin{pmatrix}-\gamma_{\rm cm}\cos\theta + \gamma_{\rm ms} - \gamma_{\rm cs}\\ \gamma_{\rm cm}\sin\theta\end{pmatrix}.\end{aligned}$$

At a steady state, the dynamic surface tension nodal force should be zero in the horizontal direction, i.e.,

$$\gamma_{\rm cs} + \gamma_{\rm cm}\cos\theta - \gamma_{\rm ms} = 0, \tag{1}$$

which is the famous Young's equation (Young 1805), relating the surface tensions between the three phases merging at the contact line $\Gamma_{\rm mcl}$. Following Gabella et al. (2014), the extra surface tension $\gamma_{\rm actin}$ induced by the active effect can be directly included in the Young's equation. The physical origin of this actin tension $\gamma_{\rm actin}$ on cell membrane is from two different cellular activities: actin polymerization and actomyosin contraction (Gabella et al. 2014; Ofer et al. 2011). Actin polymerization happens right after the onset of the late stage cell spreading, while actomyosin contraction occurs

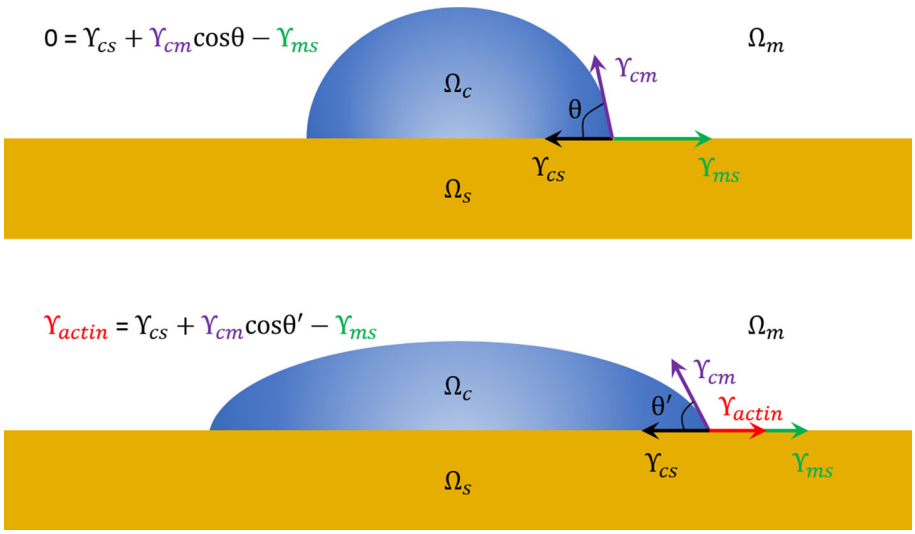

Fig. 2 Incorporating the active effects through the moving contact line

later than actin polymerization. In fact, actomyosin contraction can facilitate cellular scale actin polymerization or depolymerization during cell crawling (Wilson et al. 2010).

In this work, the actin polymerization is incorporated into the formulation through two ways: (1) the director field **h**, which will be discussed in Sect. 3, and (2) the actin tension γ_{actin} that is integrated into the surface tension force balance equation at the moving contact line (or fringe of the cell). For the sake of simplicity, in this paper, we do not consider the interaction of the two, and instead we set the actin tension γ_{actin} to be a constant during the late stage cell spreading, by assuming that the cell will spread isotropically.

With the actin polymerization or actomyosin contractile mechanism, the force balance at the moving contact line Γ_{mcl} is first broken, and then the system will reach another steady state with a new contact angle θ'. The original interphase tensions γ_{cs}, γ_{cm} and γ_{ms}, which are in general material constants, together with the active effect-induced tension γ_{actin} and the new contact angle θ', will satisfy the following balance equation:

$$\gamma_{\text{cs}} + \gamma_{\text{cm}} \cos\theta' - \gamma_{\text{ms}} = \gamma_{\text{actin}} \tag{2}$$

or

$$\gamma_{\text{cs}} + \gamma_{\text{cm}} \cos\theta' - (\gamma_{\text{ms}} + \gamma_{\text{actin}}) = 0 \tag{3}$$

In Eq. 3, the actin tension can be simply viewed as an extra contribution to the surface tension on Γ_{ms}. If the active effect-induced surface actin tension γ_{actin} is uniform along Γ_{mcl}, then one would expect the cell to spread isotropically, as shown in Fig. 2b. On the contrary, with non-uniform actin tension, one might see anisotropically movement of the cell, possibly resulting in cell crawling event. In the current work, we mainly focus on the universal dynamics of cell spreading. To model the universal spreading process, we make the following assumptions:

(1) The early stage spreading can be completely treated as a mechanical process, similar to the dynamic wetting process of a water droplet;
(2) The adhesion strength between the cell and the ECM is only dependent on the stiffness of the substrate, i.e., independent of the cell morphology or any other factors in the spreading process;
(3) In the late stages, actin polymerization and actomyosin contraction-induced actin tension is uniform and the cell spreads isotropically.

2.2 The multiscale moving contact line theory

In this part, we introduce a novel MMCL theory and its computational formulations, which are the main technical ingredient in simulations of passive cell spreading. In contrast to conventional hydrodynamics moving contact line theory, the proposed MMCL adopts the Lagrangian description. Besides, surface governing equations are taken into account, which is of great importance considering the force transmission at the contact line. At macroscopic scale, we can treat each phase of the triple-phase system by using continuum mechanics modeling, and the equation of motions of each phase are

$$\nabla_{\mathbf{x}} \cdot \boldsymbol{\sigma}_\alpha + \rho_\alpha \boldsymbol{b}_\alpha = \rho_\alpha \ddot{\boldsymbol{u}}_\alpha, \ \forall \mathbf{x} \in \Omega_\alpha, \quad \alpha = l, s, g \tag{4}$$

where $\boldsymbol{\sigma}_\alpha$ is the Cauchy stress tensor, ρ_α the density, $\boldsymbol{b}_\alpha$ the body force per unit mass and $\boldsymbol{u}_\alpha$ the displacement for each phase, correspondingly.

Here we want to point out that there are some very successful contact line models in literature that can evaluate the ability of a partial-wetting liquid in deforming the underlying substrate, notably the recently developed rival contact line models (Bostwick et al. 2014). The major contribution of the present MMCL is that it can capture the dynamic spreading process of the liquid phase over the solid substrate. In the corresponding formulas, the inertia effects are thus included in the system.

2.2.1 *Interaction forces between two distinct phases*

The MMCL theory makes use of the adhesive/contact force between the two distinct bodies to separate the cell and the ECM, i.e., it levitates the cell in the middle extracellular medium such that it removes the shear stress singularity at the conventional MCL, and the cell is free to move under the driving force of surface energy difference. During the cell spreading process, the interaction between three interphases should be considered. In our simulation, the body–body interaction between the cell and the ECM is modeled by the recent developed CGCM (Sauer and Li 2007b, a, 2008). The key technical ingredient of CGCM is to introduce an adhesive contact potential of the two bodies, based on the homogenization of molecular interaction between individual atoms or molecules. The kinematic description of two interacting bodies is shown in Fig. 3. Consider the interaction of two distinct bodies at the current configurations Ω_1 and Ω_2. The total potential energy of the whole system can be written as

$$\Pi = \sum_{I=1}^{2} \left(\Pi^{\text{int},I} - \Pi^{\text{ext},I} \right) + \Pi^{\text{ac}}, \tag{5}$$

where $\Pi^{\text{int},I}$ and $\Pi^{\text{ext},I}$ are the internal energy and external energy for body Ω_I, $I = 1, 2$. Π_{AC} denotes the homogenized interaction energy due to the interbody adhesive contact.

Suppose that there are two particles located at $\mathbf{x_1}$ and $\mathbf{x_2}$ interacting with each other via an interatomic potential ϕ,

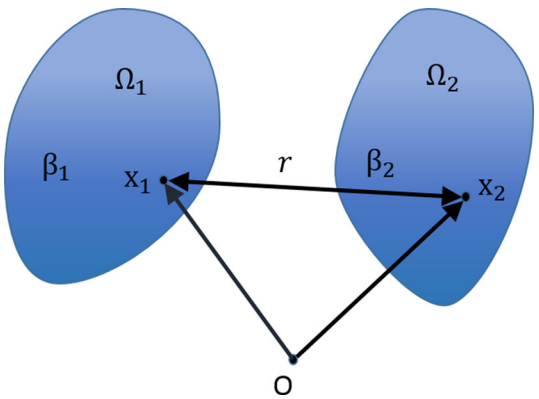

Fig. 3 The kinematics of two interacting bodies

which is a function of the current bond length $r := |\mathbf{x_1} - \mathbf{x_2}|$. $\phi(r)$ can be any potential suitable for the specific physical bonding. In this work, we use the Lennard–Jones potential, i.e.,

$$\phi(r) = \epsilon \left(\frac{\sigma_0}{r} \right)^{12} - 2\epsilon \left(\frac{\sigma_0}{r} \right)^{6}, \tag{6}$$

where ϵ is the potential well (in the unit of energy) and σ_0 is the steady-state distance. The LJ potential is chosen to represent the specific and non-specific binding forces between the cell and its ECM, and such simplified approximation has been adopted by other researchers, (Roy and Qi 2010). In the present work, we do not distinguish the cell-substrate-specific or non-specific forces (Huang et al. 2011; Sackmann and Bruinsma 2002). We would like to emphasize here that although an interacting potential of the 12-6 LJ form is chosen in the CGCM, it does not necessarily mean that our model can only simulate system in nano- or submicro-scale. This LJ potential only serves to represent the attraction or repulsion forces between the cell and the ECM. As a matter of fact, the CGCM can be employed to simulate macro scale simulations through a second-level Coarse-Graining. Interested readers can consult (Sauer 2006) for details. Moreover, one can easily switch to a different form of potential based on the present framework, if necessary. Summing up all the interbody interactions between atoms in the two bodies, one may arrive at the final form of the homogenized interaction energy for the adhesive contact

$$\Pi^{\text{ac}} = \int_{\Omega_1} \int_{\Omega_2} \beta_1 \beta_2 \phi(r) \mathrm{d}v_2 \mathrm{d}v_1, \quad r = |\mathbf{x_1} - \mathbf{x_2}|, \tag{7}$$

where β_1 and β_2 represent the current particle densities located at points $\mathbf{x_1} \in \Omega_1$ and $\mathbf{x_2} \in \Omega_2$. The first variation of the homogenized interaction energy Π_{AC} can be written as

$$\begin{aligned} \delta\Pi^{\text{ac}} &= \int_{\Omega_1} \int_{\Omega_2} \beta_1 \beta_2 \Big(\frac{\partial \phi(r)}{\partial \mathbf{x}_1} \cdot \delta \mathbf{u}_1 + \frac{\partial \phi(r)}{\partial \mathbf{x}_2} \cdot \delta \mathbf{u}_2 \Big) \mathrm{d}v_1 \mathrm{d}v_2 \\ &= - \int_{\Omega_1} \beta_1 \mathbf{b}_1 \cdot \delta \mathbf{u}_1 \mathrm{d}v_1 - \int_{\Omega_2} \beta_2 \mathbf{b}_2 \cdot \delta \mathbf{u}_2 \mathrm{d}v_2, \end{aligned} \tag{8}$$

where the body forces are defined as

$$\mathbf{b}_1(\mathbf{x}_1) := -\frac{\partial \Phi_2}{\partial \mathbf{x}_1}, \qquad \Phi_2 := \int_{\Omega_2} \beta_2 \phi(r) \mathrm{d}v_2;$$
$$\mathbf{b}_2(\mathbf{x}_2) := -\frac{\partial \Phi_1}{\partial \mathbf{x}_2}, \qquad \Phi_1 := \int_{\Omega_1} \beta_1 \phi(r) \mathrm{d}v_1.$$

For the detailed theory and the computational implementation of the CGCM, the reader may consult to (Sauer and Li 2007b, a, 2008).

The original CGCM formulation is basically a computational formulation for the body–body interaction. As shown

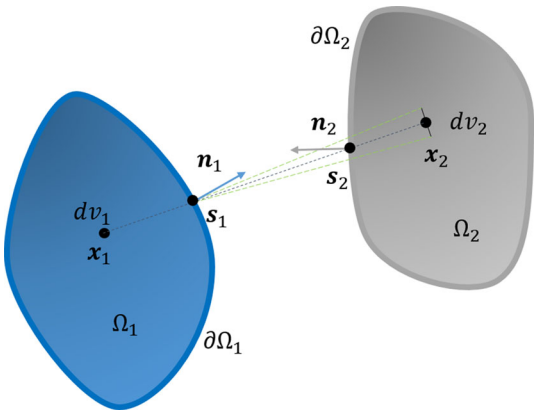

Fig. 4 A schematic for the surface–surface interaction

in Eq. (8), the body–body approach requires a double layer integration over the two deformable bodies, which is in need of great computation efforts, especially for realistic 3D simulations. Consider two bodies Ω_1 and Ω_2 interacting with each other, as shown in Fig. 4. Following the approach outlined by (Jagota and Argento 1997), we can condense the body–body interaction forces directly to a surface–surface interaction. The adhesive contact force applied on an infinitesimal surface element $da_1 \subset \partial\Omega_1$ due to the presence of an infinitesimal surface element surface $da_2 \subset \partial\Omega_2$ is expressed as,

$$d\mathbf{F}_1 = \{\beta_1\beta_2\,(\mathbf{n}_2 \otimes \mathbf{s}_{12}) \cdot \mathbf{n}_1\psi(s)\}\,da_1da_2 \tag{9}$$

where $\mathbf{n}_1$, $\mathbf{n}_2$ are the unit surface out-normal at surface points $\mathbf{s}_1$ and $\mathbf{s}_2$, respectively, and

$$\psi(s) = \frac{1}{s^3}\int_s^\infty \phi(r)r^2\mathrm{d}r, \text{ with}$$
$$s = |\mathbf{s}_{12}|, \mathbf{s}_{12} = \mathbf{s}_2 - \mathbf{s}_1 = -\mathbf{s}_{21} \tag{10}$$

For the interatomic potential $\phi(r)$ given by Eq. (6), one can easily perform the integration above and get

$$\psi(s) = \frac{2}{3}\varepsilon\left[\frac{1}{6}\left(\frac{\sigma_0}{s}\right)^{12} - \left(\frac{\sigma_0}{s}\right)^{6}\right] \tag{11}$$

Similar to Eq. (9), the adhesive contact force applied on an infinitesimal surface element $da_2 \subset \partial\Omega_2$ due to the presence of an infinitesimal surface element surface $da_1 \subset \partial\Omega_1$ is expressed as

$$d\mathbf{F}_2 = \{\beta_1\beta_2\,(\mathbf{n}_1 \otimes \mathbf{s}_{21}) \cdot \mathbf{n}_2\psi(s)\}\,da_2da_1 \tag{12}$$

2.2.2 Interface equations and surface tension effects

In the MMCL, surface tension effects are included in the triple-phase system. In addition to the conventional equations of motion in the bulk (Eq. 4), a set of surface traction boundary conditions, similar to the Gurtin–Murdoch interface formulation (Gurtin and Murdoch 1977), is considered,

$$\nabla_S \cdot \boldsymbol{\sigma}_\alpha^S + \mathbf{t}_\alpha = \rho_{s\alpha}\mathbf{a}_\alpha, \quad \alpha = l, s, g \tag{13}$$

where the subscript α denotes the corresponding quantity in each phase. $\rho_{s\alpha}$ is the surface mass density, $\boldsymbol{\sigma}_\alpha^S$ is the surface stress, $\mathbf{t}_\alpha$ is traction vector, and $\mathbf{a}_\alpha$ is the mass material acceleration. ∇_S is the surface gradient operator, defined as

$$\nabla_S := \nabla - \mathbf{n}(\mathbf{n} \cdot \nabla) \tag{14}$$

where $\mathbf{n}$ is the unit out-normal of the surface at the point of interest.

2.2.3 Galerkin weak form formulation of the MMCL theory

In this section, the Galerkin weak formulation of the MMCL theory is presented. We consider a triple system in a total Lagrange description,

$$\mathcal{L} = \sum_{\alpha=c,s,m}\left[T_\alpha - (\Pi_\alpha^{\text{int}} - \Pi_\alpha^{\text{ext}})\right] - \Pi^{\text{ac}},$$
$$\text{and} \quad \mathcal{S} = \int_{t_1}^{t_2} L\mathrm{d}t, \tag{15}$$

where $\alpha = c, s, m$ denotes the gaseous, liquid and solid phases; T_α are the kinetic energies; Π_α^{int} are the internal energies; Π_α^{ext} are the external energies; and Π^{ac} is the interaction potential energy among interphases.

Considering the least action or the stationary action principle, $\delta\mathcal{S} = 0$, we have

$$\delta\mathcal{S} = \int_{t_1}^{t_2}\delta\mathcal{L}\mathrm{d}t = \int_{t_1}^{t_2}\left\{\sum_{\alpha=c,s,m}\left[\delta T_\alpha - (\delta\Pi_\alpha^{\text{int}} - \delta\Pi_\alpha^{\text{ext}})\right] - \delta\Pi^{\text{ac}}\right\}\mathrm{d}t = 0,$$

$\forall\delta\mathbf{u}_l, \delta\mathbf{u}_s, \delta\mathbf{u}_g \in H^1(\Omega_l) \cup H^1(\Omega_s) \cup H^1(\Omega_g)$, where $\delta\mathbf{u}_l$, $\delta\mathbf{u}_s$ and $\delta\mathbf{u}_g$ are the variation of displacements in the gaseous, liquid and solid phases. The variation of the kinetic energy is given by

$$\delta T_\alpha = \int_{\Omega_\alpha}\rho_\alpha\dot{\mathbf{u}}_\alpha \cdot \delta\dot{\mathbf{u}}_\alpha\mathrm{d}v_\alpha, \ \alpha = l, s, g; \tag{16}$$

where ρ_α are the mass density in the current configuration. The variation of the internal energy is given by

$$\delta\Pi_\alpha^{\text{int}} = \int_{\Omega_\alpha}\boldsymbol{\sigma}_\alpha : \frac{\partial\delta\mathbf{u}_\alpha}{\partial\mathbf{x}}\mathrm{d}v_\alpha, \ \alpha = l, s, g. \tag{17}$$

The variation of the external energy is given as

$$\delta\Pi_\alpha^{\text{ext}} = \int_{\Omega_\alpha} \rho_\alpha \mathbf{b}_\alpha \cdot \delta\mathbf{u}_\alpha \mathrm{d}v + \int_{\partial\Omega_\alpha} \mathbf{t}_\alpha \cdot \delta\mathbf{u}_\alpha \mathrm{d}s, \quad \alpha = l, s, g, \tag{18}$$

where $\mathbf{b}_\alpha$ are the body forces and $\mathbf{t}_\alpha$ are the surface traction.

The variation of the interaction energy is given in terms of the body–body interaction method as

$$\delta\Pi^{\text{ac}} = \int_{\Omega_\alpha}\int_{\Omega_\beta} \beta_\alpha\beta_\beta \left[\frac{\partial\phi(r)}{\partial\mathbf{x}_\alpha} \cdot \delta\mathbf{u}_\alpha + \frac{\partial\phi(r)}{\partial\mathbf{x}_\beta} \cdot \delta\mathbf{u}_\beta \right] \mathrm{d}v_\beta \mathrm{d}v_\alpha, \tag{19}$$

or in terms of the surface–surface interaction method,

$$\delta\Pi^{\text{ac}} = \int_{\partial\Omega_\alpha}\int_{\partial\Omega_\beta} \beta_\alpha\beta_\beta \left\{ \left[\left(\mathbf{n}_\beta \otimes \mathbf{s}_{\alpha\beta}\right) \cdot \mathbf{n}_\alpha \psi(s) \right] \cdot \delta\mathbf{u}_\alpha + \left[\left(\mathbf{n}_\alpha \otimes \mathbf{s}_{\beta\alpha}\right) \cdot \mathbf{n}_\beta \psi(s) \right] \cdot \delta\mathbf{u}_\beta \right\} \mathrm{d}a_\alpha \mathrm{d}a_\beta \tag{20}$$

where the interphase pair $\alpha\beta : lg, gs,$ and ls.

Finally we can obtain following variational equations,

$$\int_{t_1}^{t_2} \left\{ \sum_{\alpha=c,s,m} \left[\int_{\Omega_\alpha} \rho\mathbf{v}_\alpha \cdot \delta\dot{\mathbf{u}}_\alpha \mathrm{d}v - \int_{\Omega_\alpha} \boldsymbol{\sigma}_\alpha : \frac{\partial\delta\mathbf{u}_\alpha}{\partial\mathbf{x}_\alpha} \mathrm{d}v + \int_{\Omega_\alpha} \rho_\alpha \mathbf{b}_\alpha \cdot \delta\mathbf{u}_\alpha \mathrm{d}v + \int_{\partial\Omega_\alpha} \mathbf{t}_\alpha \cdot \delta\mathbf{u}_\alpha \mathrm{d}s \right] - \int_{\Omega_\alpha}\int_{\Omega_\beta} \beta_\alpha\beta_\beta \left(\frac{\partial\phi(r)}{\partial\mathbf{x}_\alpha} \cdot \delta\mathbf{u}_\alpha + \frac{\partial\phi(r)}{\partial\mathbf{x}_\beta} \cdot \delta\mathbf{u}_\beta \right) \mathrm{d}v_\beta \mathrm{d}v_\alpha \right\} \mathrm{d}t = 0, \quad \forall\alpha\beta = lg, gs, \text{ and } ls. \tag{21}$$

or

$$\int_{t_1}^{t_2} \left\{ \sum_{\alpha=c,s,m} \left[\int_{\Omega_\alpha} \rho\mathbf{v}_\alpha \cdot \delta\dot{\mathbf{u}}_\alpha \mathrm{d}v - \int_{\Omega_\alpha} \boldsymbol{\sigma}_\alpha : \frac{\partial\delta\mathbf{u}_\alpha}{\partial\mathbf{x}_\alpha} \mathrm{d}v + \int_{\Omega_\alpha} \rho_\alpha \mathbf{b}_\alpha \cdot \delta\mathbf{u}_\alpha \mathrm{d}v + \int_{\partial\Omega_\alpha} \mathbf{t}_\alpha \cdot \delta\mathbf{u}_\alpha \mathrm{d}s \right] - \int_{\partial\Omega_\alpha}\int_{\partial\Omega_\beta} \beta_\alpha\beta_\beta \left\{ \left[\left(\mathbf{n}_\beta \otimes \mathbf{s}_{\alpha\beta}\right) \cdot \mathbf{n}_\alpha \psi(s) \right] \cdot \delta\mathbf{u}_\alpha + \left[\left(\mathbf{n}_\alpha \otimes \mathbf{s}_{\beta\alpha}\right) \cdot \mathbf{n}_\beta \psi(s) \right] \cdot \delta\mathbf{u}_\beta \right\} \mathrm{d}a_\alpha \mathrm{d}a_\beta \right\} \mathrm{d}t = 0, \quad \forall\alpha\beta = lg, gs, \text{ and } ls. \tag{22}$$

This is the Galerkin weak form of the MMCL Theory. Note that in Eq. (22), the traction force $\mathbf{t}_\alpha$ on $\partial\Omega_\alpha$ does not include the adhesive traction due to the Derjaguin approximation. If we absorb the adhesive traction force into $\mathbf{t}_\alpha$, the weak form is then simplified as the conventional expression,

$$\int_{t_1}^{t_2} \left\{ \sum_{\alpha=c,s,m} \left[\int_{\Omega_\alpha} \rho\mathbf{v}_\alpha \cdot \delta\dot{\mathbf{u}}_\alpha \mathrm{d}v - \int_{\Omega_\alpha} \boldsymbol{\sigma}_\alpha : \frac{\partial\delta\mathbf{u}_\alpha}{\partial\mathbf{x}_\alpha} \mathrm{d}v + \int_{\Omega_\alpha} \rho_\alpha \mathbf{b}_\alpha \cdot \delta\mathbf{u}_\alpha \mathrm{d}v + \int_{\partial\Omega_\alpha} \mathbf{t}_\alpha \cdot \delta\mathbf{u}_\alpha ds \right] \right\} \mathrm{d}t = 0. \tag{23}$$

For the sake of simplicity, details of the FEM discretization are omitted. Here, we only provide the formulation of the traction boundary condition to the surface force on the nodes at the boundary $\partial\Gamma_l$,

$$\mathbf{F}_l^s = -\sum_{I_s=1}^{N_{\text{Snode}}} \left\{ \int_{\Gamma_{\text{cs}}} \frac{\partial N_{I_s}}{\partial\mathbf{x}} : \boldsymbol{\sigma}_{\text{cs}}^S \mathrm{d}s + \int_{\Gamma_{\text{cm}}} \frac{\partial N_{I_s}}{\partial\mathbf{x}} : \boldsymbol{\sigma}_{\text{cm}}^S \mathrm{d}s + \int_{\Gamma_{\text{ms}}} \frac{\partial N_{I_s}}{\partial\mathbf{x}} : \boldsymbol{\sigma}_{\text{ms}}^S \mathrm{d}s \right\}. \tag{24}$$

where N_{Snode} is the total number of surface element nodes and $N_{I_s}(\mathbf{x})$ are the surface finite element shape functions. Readers interested on how to obtain Eq. (24) may consult (Minaki and Li 2014) for the details.

2.3 Constitutive modelings

The constitutive modelings for the nematic droplet, the elastic substrate and its corresponding surface elasticity are discussed in following sections.

2.3.1 Modeling cells as active nematic droplets

In this work, we adopt the constitutive equation from (Edwards and Yeomans 2009) in simulations of the nematic flow. The presence of nematic order in cells is because of the polarity field of F-actin filament. In fact, F-actin itself is a nematic liquid polymer solution (Viamonte et al. 2006; Viamontes and Tang 2003), i.e., each F-actin monomer has a plus end and a minus end, and the actin monomers all orient with their cleft toward the minus end of the actin filament, which is responsible for many cellular functions and motilities, such as treadmilling, contractile force and retrograde flow.

The Cauchy stress in the active nematic model of the aggregated actin filament is given as follows,

$$\boldsymbol{\sigma} = \kappa \ln(J)\mathbf{1} + 2\mu\mathbf{d} + \frac{\lambda}{2}(\boldsymbol{h}\otimes\boldsymbol{s} + \boldsymbol{s}\otimes\boldsymbol{h}) - \frac{1}{2}(\boldsymbol{h}\otimes\boldsymbol{s} - \boldsymbol{s}\otimes\boldsymbol{h}) - \xi\mathbf{h}\otimes\mathbf{h} \tag{25}$$

where κ is the bulk modulus of the cell; μ is the viscosity; $\mathbf{d}$ is the rate of deformation tensor; $\mathbf{h}$ is a director field that mimics the nematic order of F-actin filaments at coarse grain level; $\boldsymbol{s} = -\eta\nabla^2\boldsymbol{h}$ is the molecular field conjugate to the director field (Edwards and Yeomans 2009); and λ, η are positive

constants. The last term in Eq. (25) i.e., $-\xi \mathbf{h} \otimes \mathbf{h}$ is the so-called active stress term. It provides modeling of prestress and energy input during F-actin polymerization from isotropic G-actins by ATP hydrolysis (Joanny and Prost 2009). The active stress term, $-\xi \mathbf{h} \otimes \mathbf{h}$, may also provide a contractile force that can generate internal treadmilling for actin cytoskeletons. This is because that the active stress term is the contribution from a dipolar force generated by the director field. In all the calculations done in the work, we choose $\xi = 1.0 \times 10^{-5}$ Pa.

The Cauchy stress defined in Eq. (25) is a nonstandard Cauchy stress. Besides the displacement field $\boldsymbol{u}$, the Cauchy stress inside the nematic droplet is also dependent on the director field $\boldsymbol{h}$, and it is asymmetric. Thus, in order to solve the equations of motion for the nematic droplet, extra governing equations for the director field are needed. In our simulation, these governing equations for the director field $\boldsymbol{h}$ are based on that of (Edwards and Yeomans 2009; Joanny and Prost 2009), except that we add a Landau–Ginzburg type of potential as a free energy, which serves as a penalty to regulate the magnitude of the director field,

$$\frac{D\tilde{\boldsymbol{h}}}{Dt} = \gamma \{\nabla \cdot (\nabla \otimes \boldsymbol{h}) - \boldsymbol{r}(\boldsymbol{h})\} - \nu_1 \mathbf{d}\boldsymbol{h} - \nu_2 tr(\boldsymbol{\ell})\boldsymbol{h}, \quad \forall \mathbf{x} \in \Omega_1(t) \tag{26}$$

where

$$\boldsymbol{\ell} = \dot{\mathbf{F}}\mathbf{F}^{-1}, \text{ and } \mathbf{d} = \frac{1}{2}(\boldsymbol{\ell} + \boldsymbol{\ell}^T) \tag{27}$$

and $\mathbf{F}$ is the deformation gradient, $\boldsymbol{v} = v_i \boldsymbol{e}_i$ is the velocity field, γ is the director elastic constant, and ν_1 and ν_2 are positive constants. $\boldsymbol{r}$ is the force vector resulting from the Landau–Ginzburg type free energy,

$$\boldsymbol{r} = \frac{\mathrm{d}R(\boldsymbol{h})}{\mathrm{d}\boldsymbol{h}} = \frac{\boldsymbol{h}}{\epsilon^2}(\|\boldsymbol{h}\|^2 - 1), \text{ and } R(\boldsymbol{h}) = \frac{1}{4\epsilon^2}(\|\boldsymbol{h}\|^2 - 1)^2 \tag{28}$$

One may note that in Eq. (26), a corotational convected time rate $\frac{D\tilde{\boldsymbol{h}}}{Dt}$ is used, which is very important for large deformation dynamic computations, because it ensures the objectivity of time integration. In this work, we set

$$\frac{D\tilde{\boldsymbol{h}}}{Dt} = \frac{D\boldsymbol{h}}{Dt} + \boldsymbol{\ell}^T \boldsymbol{h}. \tag{29}$$

2.3.2 Constitutive equations of the ECM

For the extracellular matrix, we use the St. Venant–Kirchhoff material model (see Holzapfel 2000). It is a full nonlinear model in the displacements, and thus it can be used for large displacement calculations with a formulation similar to small strain case. The free energy density function is given as

$$W(\mathbf{E}) = \frac{\lambda}{2}(\mathrm{tr}\mathbf{E})^2 + \mu \mathrm{tr}\mathbf{E}^2, \tag{30}$$

where $\mathbf{E}$ is the Green–Lagrange strain tensor and λ and μ are the Lame constants. The second Piola–Kirchhoff stress tensor $\mathbf{S}$ can then be derived as

$$\mathbf{S} = \frac{\partial W}{\partial \mathbf{E}} = \lambda (\mathrm{tr}\mathbf{E})\, \mathbf{I} + 2\mu \mathbf{E} \tag{31}$$

where $\mathbf{I}$ is the unit second-order tensor in 3D space.

2.3.3 Surface elasticity

Without considering surface diffusion and friction, the following surface constitutive relations are chosen,

$$\boldsymbol{\sigma}_m^S = \gamma_m \mathbf{I}_S^{(2)} \tag{32}$$

$$\boldsymbol{\sigma}_c^S = \gamma_c \mathbf{I}_S^{(2)} + \nabla_S \gamma_c \mathbf{I}_S^{(2)} + \frac{\mu_S}{2}\left(\nabla_S \otimes \mathbf{v} + (\nabla_S \otimes \mathbf{v})^T\right) \tag{33}$$

$$\boldsymbol{\sigma}_s^S = \gamma_s \mathbf{I}_S^{(2)} + \frac{\partial \Gamma_S}{\partial \boldsymbol{\epsilon}^S} + \gamma_s \nabla_S \otimes \mathbf{u}. \tag{34}$$

where $\mathbf{u}$ and $\mathbf{v}$ are displacement and velocity fields; μ_S is the surface viscosity; γ_s, γ_c and γ_m are the surface tension in different phases; Γ_S is the solid surface strain energy; $\boldsymbol{\epsilon}^S$ is the surface strain tensor; ∇_S is the surface gradient operator defined in Eq. (14); and the operator $\otimes$ is the standard notation for tensor product in tensor algebra or analysis. Finally, we use the symbol, $\mathbf{I}_S^{(2)}$, to denote the unit second-order tensor in tangent space of the surface or interface.

For the case of infinitesimal deformation, Gurtin and Murdoch proposed the following quadratic form of the surface strain energy (Gurtin and Murdoch 1977),

$$\Gamma_S = \frac{1}{2}\epsilon^S{}_{ij} C^S_{ijkl} \epsilon^S{}_{kl}, \quad i, j, k, l = 1, 2 \tag{35}$$

in which the surface elastic tensor is related to surface tension γ_S as well,

$$C^S_{ijkl} = \left(\lambda^S + \gamma_s\right)\delta_{ij}\delta_{kl} + \mu^S\left(\delta_{ik}\delta_{jl} + \delta_{il}\delta_{jk}\right), \quad i, j, k, l = 1, 2 \tag{36}$$

where λ^S and μ^S are the surface Lame constants. Hence, the surface constitutive equations for the solid phase become

$$\boldsymbol{\sigma}_s^S = \gamma_S \mathbf{I}_S^{(2)} + 2\left(\mu^S - \gamma_s\right)\boldsymbol{\epsilon}^S + \left(\lambda^S + \gamma_s\right) tr(\boldsymbol{\epsilon}^S)\mathbf{I}_S^{(2)} + \gamma_s \nabla_S \otimes \mathbf{u} \tag{37}$$

Subsequently, one can readily derive the interface constitutive relation, for instance,

$$\begin{aligned}\boldsymbol{\sigma}^S_{\mathrm{cs}} &= \gamma_{\mathrm{cs}}\mathbf{I}_S^{(2)} + \nabla_S\gamma_c\mathbf{I}_S^{(2)} + 2\left(\mu^S - \gamma_s\right)\boldsymbol{\epsilon}^S \\ &\quad + \left(\lambda^S + \gamma_s\right) tr(\boldsymbol{\epsilon}^S)\mathbf{I}_S^{(2)} + \gamma_s\nabla_S \otimes \mathbf{u} \\ &\quad + \frac{\mu_S}{2}\left(\nabla_S \otimes \mathbf{v} + (\nabla_S \otimes \mathbf{v})^T\right)\end{aligned} \tag{38}$$

where the surface strain $\boldsymbol{\epsilon}^S$ is determined by projecting the bulk strain onto the local tangent space of the surface, i.e.,

$$\boldsymbol{\epsilon}^S := \mathbf{P}\cdot\boldsymbol{\epsilon}\cdot\mathbf{P} \tag{39}$$

Note that $\mathbf{I}_S^{(2)}$ denotes the unit tensor in the tangent space of a smooth surface or two-dimensional manifold, which is defined as

$$\mathbf{I}_S^{(2)} := \mathbf{P}\mathbf{I} = \mathbf{P}, \tag{40}$$

where $\mathbf{I}$ is the unit tensor in a 3D Euclidean space and $\mathbf{P}$ is the projection tensor defined as

$$\mathbf{P} := \mathbf{I} - \mathbf{n}\otimes\mathbf{n}, \tag{41}$$

where $\mathbf{n}$ is the unit out-normal of the surface at the point of interest. In some part of the text, in order to emphasize the material properties of the manifold, we write it as $\mathbf{I}_S^{(\alpha)}$, $\alpha = c, s, m$ or cs, ms and cm etc., in a manner that is self-evident. One may note that

$$\nabla_S\cdot\mathbf{I}_S^{(2)} = \nabla_S\cdot\mathbf{P} = 2\kappa\mathbf{n} \tag{42}$$

where κ is the local mean curvature of the surface.

2.4 Force dipole field and the corresponding distributed moment

Because of the presence of the director field, which is the mesoscale representation of the polarized actin filaments, the Cauchy stress tensor is no longer symmetric (see Eq. 25). This will lead to a local force dipole distribution inside the cell. We can calculate the force dipole moment inside a cell as

$$\mathbf{m} = \epsilon_{ijk}\sigma_{jk}\mathbf{e}_i \tag{43}$$

where ϵ_{ijk} is the permutation symbol. To investigate the effect from the interaction between the cell and the substrate, we define the dipole moment field as

$$\mathbf{p}(\mathbf{x}, t) = \mathbf{m}(\mathbf{x}, t) - \mathbf{m}_0(\mathbf{x}). \tag{44}$$

where $\mathbf{m}_0$ is the initial dipole moment field induced by prestress.

For simplicity, we choose an initial state so that the initial direction of the director field is along the radical direction, i.e., $\mathbf{h}(\mathbf{x}, 0) = \mathbf{n}(\mathbf{x}, 0) = \mathbf{n}_0(\mathbf{x})$. In fact, by doing so, the prestress state due to the initial director field $\mathbf{h}(\mathbf{x}, 0)$ is purely dilatational and hence $\mathbf{m}_0 = \mathbf{0}$. In this case, one may find the initial molecular field,

$$\mathbf{s}_0 = -\frac{\eta}{r^2}\mathbf{h}_0 \tag{45}$$

where r is the radial distance between the center of the droplet to the point under consideration. Under this condition, the polarization field is the dipole moment field, i.e., $\mathbf{p} = \mathbf{m}$. During the spreading of the cell over the elastic substrate, we can calculate the projection of the polarization vector onto the original director filed axis $\mathbf{n}$,

$$\cos\bar{\theta} := \bar{\mathbf{p}}\cdot\mathbf{n}, \quad \bar{\mathbf{p}} := \frac{\mathbf{p}}{|\mathbf{p}|}, \tag{46}$$

where $\mathbf{n}(\mathbf{x})$ is the direction of the local nematic axis, and it may be interpreted as the chosen direction of the actin stress fiber. In this paper, we name $\cos\bar{\theta}$ as the orientation order parameter.

3 Numerical examples

3.1 Dynamic spreading of a living cell

In this section, the simulation of a living cell spreading upon the ECM is presented. The cell is modeled as a nematic droplet, while the ECM is treated as an elastic substrate. The cell was initially in suspension and placed above the elastic substrate, as shown in Fig. 5a. We have carried out the simulation, attempting to capture the different features at different stages of the spreading process, i.e., early stage spreading (Fig. 5b) and the late stage spreading (Fig. 5c). As indicated in the three assumptions made in Sect. 1, only physical interactions among the cell, the ECM and the extracellular medium are considered for early stage spreading. We expect that the cell will show a weak contact/adhesion on the substrate, resembling a "ball-up" phenomena. In the late stage, an actin tension force γ_{actin} is introduced, applying at the moving contact line, parallel to the ECM surface, as shown in Fig. 5c. Due to the effect of the actin polymerization and/or actomyosin contraction, the cell will then spread over the substrate.

Initially, the cell is set as a perfect sphere with a radius $r = 5\ \mu\mathrm{m}$, which is discretized into 4000 eight-node brick elements with 4341 nodes. The elastic substrate is a thick cylinder plate with the dimension $H = 4.75\ \mu\mathrm{m}$, $R =$

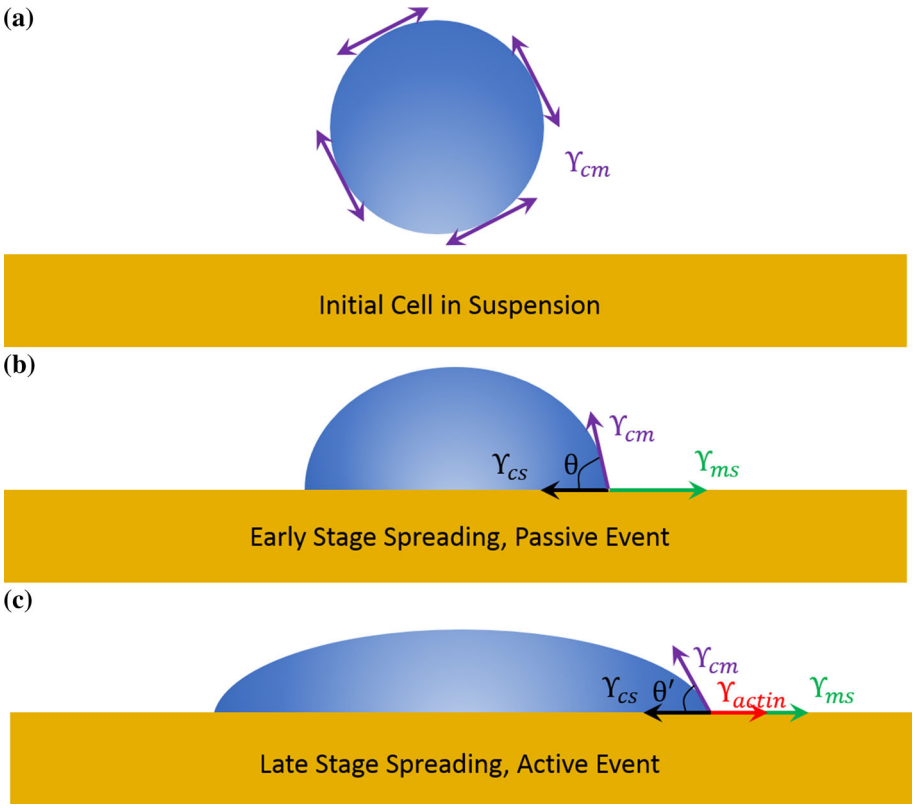

Fig. 5 Illustration of different stages of a spreading cell

20.0 μm, which is discretized into 2916 eight-node brick elements with 4036 nodes. The computational model is shown in Fig. 6. The material properties of the cell and the simulation-related constants are: density $\rho_c = 1.0\times10^3$ kg/m^3, viscosity $\mu = 1.0 \times 10^{-2}$ Pa s, bulk modulus $\kappa = 2.2 \times 10^8$ Pa, $\eta = 5.0 \times 10^{-8}$, $\nu_1 = 2.0$, $\nu_2 = 2.0$, $\epsilon = 1.0 \times 10^{-4} and\ \gamma = 1.0\times10^{-4}$. The material parameters for the St. Venant Kirchhoff elastic substrate are density $\rho_s = 1.0 \times 10^3$ kg/m^3, Young's modulus $E = 220$ KPa and Possion's ratio $\nu = 0.493$. Most of these parameters are taken from (Zeng and Li 2011a), other than the two coefficients ν_1 and ν_2, which are chosen according to (Julicher et al. 2007). The Lame constants can be obtained by

$$\lambda = \frac{\nu E}{(1+\nu)(1-2\nu)} \tag{47}$$

$$\mu = \frac{E}{2(1+\nu)}. \tag{48}$$

The atomic densities are set to be that of water $\beta_c = \beta_s = 3.3 \times 10^{28}/\text{m}^3$. The surface tensions between the three different phases are chosen according to the average membrane tension (8.0×10^{-2} N/m) and the contact angle of the cell (60°) (Hategan et al. 2003): the cell and the extracellular medium $\gamma_{\text{cm}} = 7.28 \times 10^{-2}$ N/m; the cell and the extracellular matrix $\gamma_{\text{cs}} = 1.35 \times 10^{-2}$ N/m; the cell extracellular

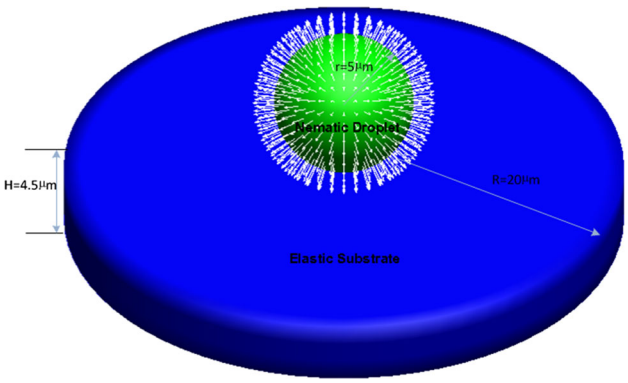

Fig. 6 Computational model of the nematic droplet and the elastic substrate

matrix and extracellular medium $\gamma_{\text{ms}} = 9.85 \times 10^{-1}$ N/m; the actin tension $\gamma_{\text{actin}} = 6.3 \times 10^{-2}$ N/m. In our simulation, we do not distinguish specific or non-specific forces between the cell and the substrate. The other coarse-grained parameters of the adhesive contact are given as $\sigma_0 = 1$ μm, $\varepsilon = 5.0 \times 10^{-16}$ J, which usually results in an average gap of 400 nm between the cell and the elastic substrate. We would like to point out that the adhesive strength ε is chosen according to the magnitude of the surface tensions, material properties of the cell and the substrate (stiffness in particular), such that the cell can successfully adhere to the substrate and

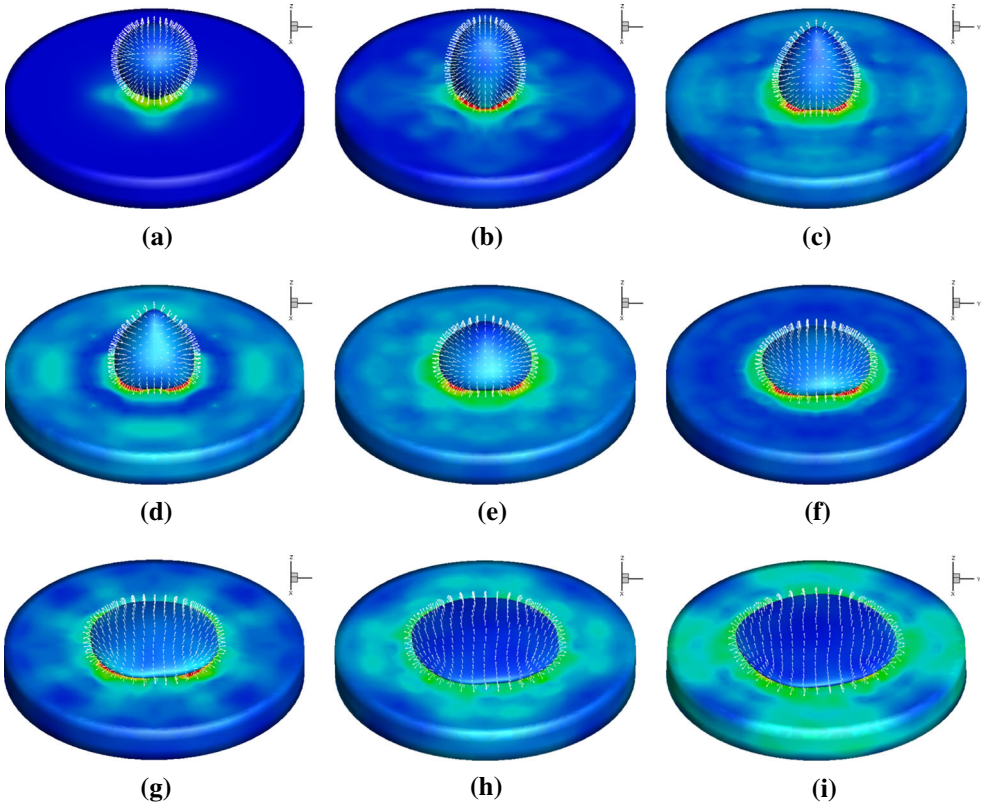

Fig. 7 Temporal evolution of the cell spreading over an elastic substrate. **a** $t = 0.04t_0$, **b** $t = 0.08t_0$, **c** $t = 0.24t_0$, **d** $t = 0.32t_0$, **e** $t = 0.4t_0$, **f** $t = 0.48t_0$, **g** $t = 0.64t_0$, **h** $t = 0.72t_0$, **i** $t = 0.8t_0$

spread over on it once the actin tension is involved, within an acceptable amount of simulation time. During the simulation process, the bottom part of the substrate is fixed. The cell is prescribed with the prescribed director field boundary condition, i.e., the director $\boldsymbol{h}$ in the out-layer of the droplet is fixed in out-normal direction of the surface. The choice of this essential boundary for the director field is based on the mechanical structure of the cell membrane, which is a lipid-bilayer.

Figure 7 presents a time sequence of snapshots of the cell spreading process. The simulation time step is $dt = 1.25 \times 10^{-10}$ s, with a total amount of time $t_0 = 20$ μs. The total simulation time is not sufficient for a real cell to completely spread (Hategan et al. 2004). The computational cost for simulation of a complete cell spreading process is so large that we have to choose a larger adhesive strength ε, which might be viewed as an acceleration factor (like in the steered molecular dynamics, Izrailev et al. 1999) to speed the computation process, so as to mimic the real cell spreading. To capture the dynamic spreading process as a whole, we divide the total simulation time into two parts. The first part is pure mechanical, by which we mean that the cell is treated as a passive object. In the second part, the actin tension γ_{actin} is applied at the MCL. The steady-state shapes of the cell at the end of each part are shown in Fig. 7e, i, respectively. We would like to mention the importance of the role the actin tension force γ_{actin} played in the spreading process. As can be seen from Fig. 7, the cell first adheres to the substrate (a–d), guided by the contact/adhesion force from the CGCM, resembling the "ball-up" shape. Without the effect of the actin tension, the cell would stay there, with no further spreading. At the moving contact line Γ_{mcl} of the triple phase system, a net force parallel to the surface of the substrate, pointing to, approximately, the out-radius direction of the cylinder, is applied to the fringe of the cell. Thus, the cell continues spreading till another steady state is achieved (see Fig. 7e–i). The MMCL is highly dependent on the contact model, and one is always required to detect the current location of moving contact line. It is this MMCL model, combined with the treatment of the actin tension effects that makes the spreading possible for the cell spreading on the substrate. The spreading areas are measured during the simulation, and they are compared with experimental observation. In our simulation, the spreading area is calculated and obtained based on the position of the moving contact line front. Due to the discrete feature of finite element method, the MCL is approximated by the surface element edges of the cell. The positions of the moving contact lines are obtained using a surface-to-surface contact detection algorithm, which is omitted here in order to focus on the content of cell mechanics. Figure 8 shows several examples

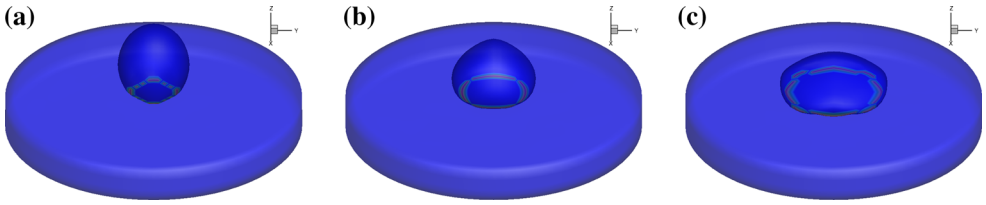

Fig. 8 MCLs at three different instances during the cell spreading process, the *red rings* in the fringes of the contact regions represent the MCLs: **a** early stage soft contact/adhesion, **b** intermediate stage of spreading, **c** late stage of spreading

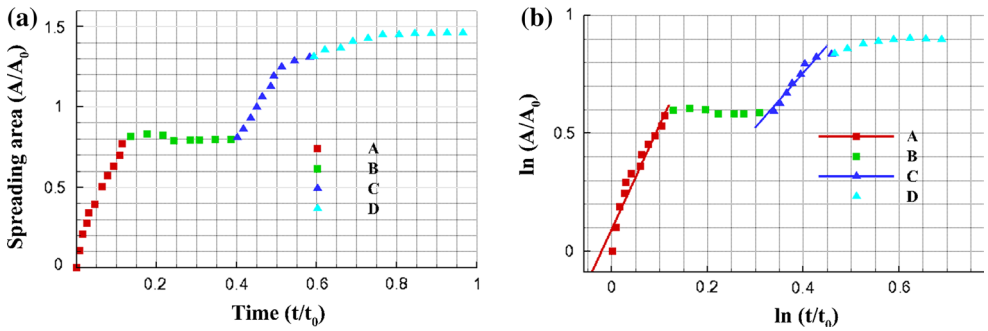

Fig. 9 Temporal evolution of the cell spreading area over the elastic substrate. The units are $A_0 = 78.54\,\mu\text{m}^2$ and $t_0 = 20\,\mu\text{s}$. **a** Spreading area A versus simulation time t. **b** loglog plot, $\ln(A/A_0)$ versus $\ln(t/t_0)$

of the MCLs in the spreading process. Using the coordinates of the nodes at the MCL, one can readily obtain the average radius of the contact region and hence the spreading area.

Figure 9 shows the spreading area versus time evolution of the entire process. Initially, the long-range attractive force between the cell and the substrate drives the rapid spreading of the cell (A). A steady state is reached (B) through the balance between the forces from the contact/adhesion and the passive surface tensions. The early stage spreading process corresponds to the range $t = 0$ to $t = 0.12t_0$ in the figure. With the introduction of the actin tension γ_{actin}, the early stage steady state is broken, and the system will reach a new steady state (D), with the increase in the spreading area (C). The late stage spreading starts from $t = 0.40t_0$. The spreading of cells over elastic substrates has been studied by many researchers (Cuvelier et al. 2007; Dobereiner et al. 2004; Douezan et al. 2011; McGrath 2007; Sun et al. 2009; Vernerey and Farsad 2014; Wolfenson et al. 2014). It is found that the evolution of contact radius follows specific power laws, for a wide range of cell types and substrates. In particular, Cuvelier et al. (2007) demonstrates from experiments that for early stage cell spreading, the contact radius versus spreading time follows a square root law $\sqrt{A} \sim \sqrt{t}$ or $A \sim t$, where A is the spreading area and t is the spreading time. Li et al. (2014) and Chamaraux et al. (2005) show that the power law relations do not even dependent on the time scale of the spreading process (Chamaraux et al. 2005; Li et al. 2014).

As can be seen from Fig. 9a, the temporal evolution of the cell spreading area approximately follows the trend $A \sim t$ in the early stage. For better illustration, a log–log plot of the spreading area versus time curve is shown in Fig. 9b. Both the early stage (A) and late stage (C) are well fitted by straight lines, which indicates both the early stage and the late stage cell spreading satisfy the power laws. We want to make a remark on the late stage spreading that the isotropic spreading behavior lies in the assumption that the actin polymerization or actomyosin contraction-induced actin tension is uniform around the moving contact line Γ_{mcl}. In reality, this is not always the case. In fact, we believe that a specific asymmetrical actin tension effect resulting from actin polymerization or actomyosin induced might lead to the cell crawling phenomenon.

3.2 Investigation of the cell mechanotransduction and the force dipole field

In this section, cell spreading simulations over substrate with various stiffness are studied, in an attempt to probe the mechanotransduction due to the interaction between the cell and the extracellular environment. Here it is assumed that the adhesion strength is larger in substrate with higher Young's modulus (Huang et al. 2011; Lo et al. 2000). The potential wells of the three coarse-grained potentials, which characterize the surface and interface energies of three substrates, are chosen as $\varepsilon_I = 2.0 \times 10^{-16}$ J, $\varepsilon_{II} = 5.0 \times 10^{-16}$ J and $\varepsilon_{III} = 1.0 \times 10^{-15}$ J. Other material parameters used in the simulations for the cell are the same as those in the previous example. We set $E_0 = 20$ KPa, $\nu_0 = 0.493$ as the base Young's modulus value, and the Young's modulus for the three different substrates is subsequently represented as

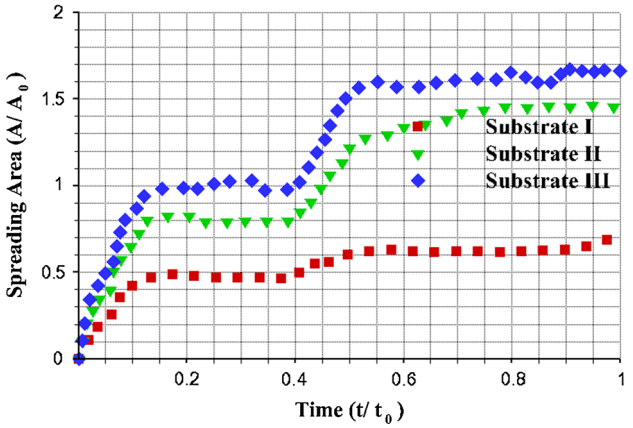

Fig. 10 Temporal evolutions of the cell spreading areas over various elastic substrates. The units are $A_0 = 78.54\,\mu\text{m}^2$ and $t_0 = 20\,\mu\text{s}$

$$\text{Substrate I}: \quad E^{S_I} = 2E_0;\ \nu^{S_I} = \nu_0 \tag{49}$$

$$\text{Substrate II}: \quad E^{S_{II}} = 5E_0;\ \nu^{S_{II}} = \nu_0 \tag{50}$$

$$\text{Substrate III}: \quad E^{S_{III}} = 10E_0;\ \nu^{S_{III}} = \nu_0 \tag{51}$$

where E denotes the Young's modulus and ν is the Possion's ratio. The relationship between spreading area versus time for the three different substrates is given in Fig. 10. It reveals that the stiffer the substrate, the more (large area) the cell spreads (see Fig. 11). Despite the similar spreading trend, at the same instance, the spreading areas of the cell on the three different substrates are quite different. Specifically, for a fixed instant, the stiffer the substrate, the larger the spreading area, which is in good agreement with results reported in literature.

To study the internal dipole moment field inside the cell, we make horizontal cuts of the cell at different heights, with the cutting plane parallel to the XOY surface (substrate surface). Figure 12 shows the distributions of the orientational order parameters for the dipole moment field of a same cell spreading over three substrates with different elastic stiffnesses. One may find that the distributed dipole moment field seems to exert torques on the center area of the droplet, where the cell nucleus is supposed to reside. A recently study by Kumar et al. (2014) on the rotation of the nucleus by actomyosin contractility must be mentioned here (Kumar et al. 2014), in which it is found in the experiment and explained in numerical simulation through a hydrodynamics modeling that actomyosin contractility plays a crucial role in the phenomenon of nuclear rotation. By comparing the numerical model in the present work with that in Kumar et al. (2014), we find that there are several similarities. First, both models consider a director field, which is assumed to be a unit vector attached to each material point. Second, the evolution of the director field is related to the symmetric and antisymmetric of the velocity gradient. And third, the total Cauchy stress tensors are the same. One can see that the stress tensor in Eq. (25) or the corresponding one in Kumar et al. (2014) is in general asymmetric, leading to a distributed dipole moment at each material point in the system. It is possible that the active stress term speeds up the rotational process, but from the mechanical point of view, we believe that the most direct reason for rotation is the distributed dipole moment or torque. In the present work, the substrate stiffness and the adhesive strength are correlated. For a higher stiffness, the adhesive strength is larger. At the same time instance, the cell on the three different substrates will have different stress distributions. As one would expect, for the substrate with higher stiffness, the stress is in general larger in magnitude, leading to a larger distributed moment or torque in the cell and hence the distinct pattern of the orientational order parameter. Overall, this observation implies that: (1) Substrate elasticity can activate and then transduce dipole moment distribution inside the cell, which may provide an overall or effective signaling pathway for mechanotransduction other than the specific molecular cellular signaling pathways, and (2) The distinct distribution pattern of the order parameter may provide a viable measurement or quantification for mechanotransduction of substrate elasticity.

4 Discussions

Despite the fact that cell spreading is a fundamental biological process that plays a key role in many important cellular behaviors, investigations on the spreading of living cells are mainly conducted through experiments (Dubin-Thaler et al. 2008; Fardin et al. 2010; Li et al. 2014; McGrath 2007; Vianay et al. 2010). Although some phenomenological cell models have been developed at continuum level (Karcher et al. 2003; Sun et al. 2009; Vernerey and Farsad 2011a, b),

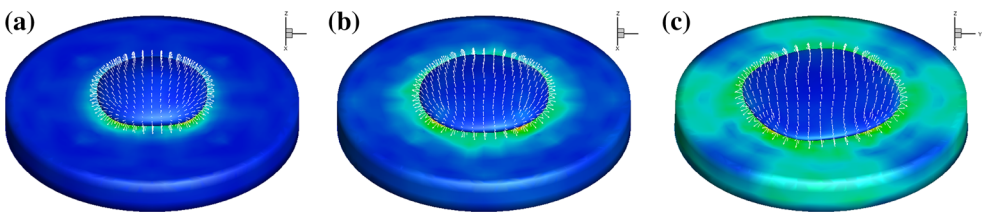

Fig. 11 Final state of a cell spreading over substrates with different stiffness: **a** Substrate I, **b** Substrate II, **c** Substrate III

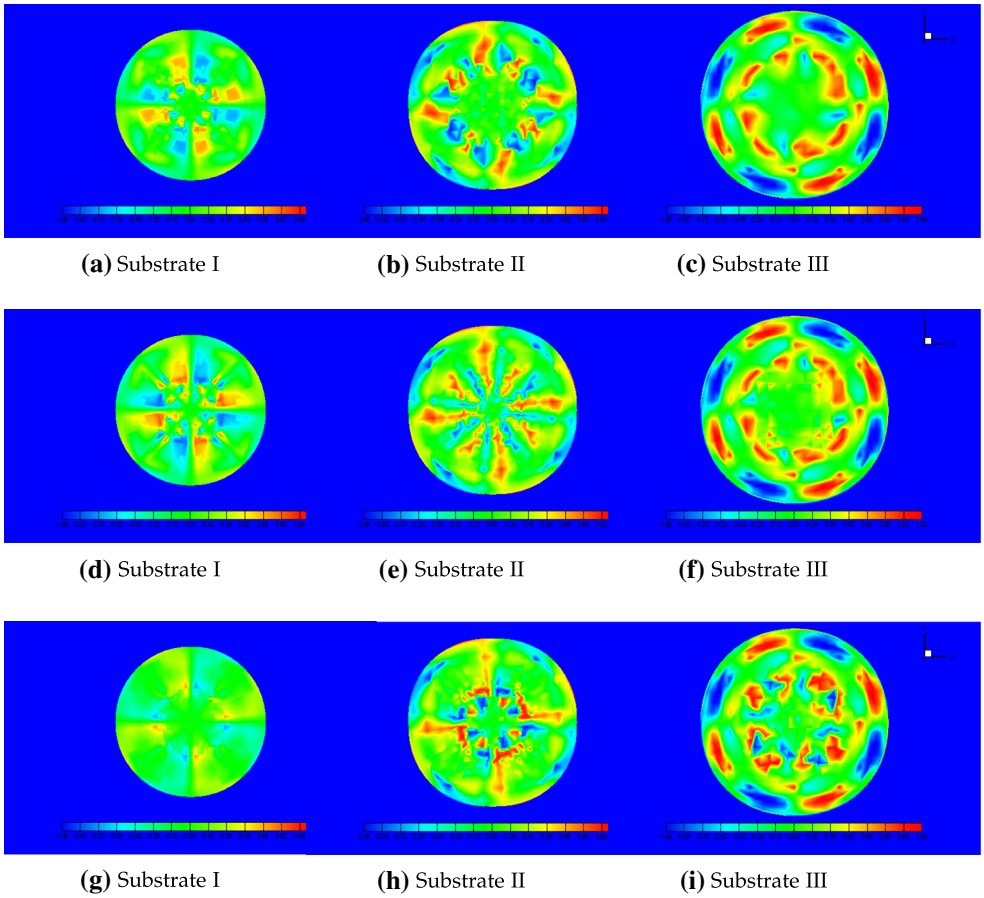

(a) Substrate I **(b)** Substrate II **(c)** Substrate III

(d) Substrate I **(e)** Substrate II **(f)** Substrate III

(g) Substrate I **(h)** Substrate II **(i)** Substrate III

Fig. 12 Horizontal views of the orientational order parameter distribution $\cos\bar{\theta}(\mathbf{x})$ in a deformed droplet for three different substrates, with the section distances to the substrates as 1500 nm above the substrate (**a**–**c**), 1000 nm above the substrate (**d**–**f**), 500 nm above the substrate (**g**–**i**)

there are very few soft matter cell models that can directly simulate 3D cell spreading based on the intrinsic characteristics of living cells.

In this work, a novel MMCL theory is developed and combined with a soft matter cell model. The MMCL theory is a Lagrange-based continuum model that can be used to simulate dynamic droplets spreading over elastic substrates, using a coarse-grained contact algorithm and the Gurtin–Murdoch surface elasticity theory, which levitates the droplet above the substrate, so that it can spread under the surface energy difference. By incorporating the actin tension effect resulting from actin polymerization or actomyosin contraction, the cell spreading simulations are carried out under specific assumptions in different stages.

It is revealed that the present soft matter cell model can successfully simulate cell spreading over elastic substrates. In particular, the temporal evolutions of the cell spreading area followed the experimentally observed specific power laws in different spreading stages. The early stage spreading is a passive spreading process, and our assumption that no actin tension effect exists may be valid, according to the literature. As for the late stage spreading, we assumed that both the actin polymerization and actomyosin contraction-induced tension effects are isotropic, which may not always be the case, especially for the contraction part. It is the combination of the actin polymerization and actomyosin contraction that leads to cell crawling phenomenon. In fact, we believed that with the introduction of certain asymmetrical actin tension effect, one may be able to quantitatively study the cell crawling phenomenon from a numerical perspective.

In addition to the universal cell spreading law, investigations on the effect of substrate stiffness on the cell spreading area as well as the dipole moment distributions inside the cell are also performed. It is found that for a fixed time duration, the stiffer the substrate, the larger the final spreading area. The patterns of the order parameter seem to indicate that the distributed moment field actually exerted torques on the center of the cell, which might provide a viable measurement for mechanotransduction of substrate elasticity.

It should be noted that the behaviors of cells are complex biological phenomena. The proposed soft matter cell model is only intended to model mechanical behaviors of cells at mesoscale level, which may not and cannot explain the molecular mechanisms of cellular processes such as cell

division or proliferation. A complete understanding the molecular mechanism of the cellular process requires an in-depth study of every aspects of molecular cell biology including all relevant biochemical, biophysical, as well as biomechanical factors and their interactions at different scales.

Nevertheless, developing active soft matter models for cells may help us understand mechanobiology of cells. It has been shown in this work that the soft matter cell model may offer a unique approach that is sound in thermodynamics and statistical biomechanics, and it provides much more insights on interaction between the cell and its mechanical niche than that of conventional hyperelastic or viscoelastic cell models. In some cases, the soft matter model has even shown its predictive power, such as cellular morphology change and the origin of cell motility (Zeng and Li 2011a, b, 2012).

Overall, the proposed model provides a unified framework for understanding the universal cell spreading by focusing on the collective aspects of the cell whose behavior is determined by its coarse-grained microstructure and material properties. It is worth mentioning that there are a variety of different molecular based cellular models, which suggests that a macroscopic model that focuses on the collective material properties of the cell may be sufficient to explain experimental data. The predictive ability of the present soft matter cell model may provide both scientific insight and clinic guidance to many of healthcare problems, such as regenerated medicine and drug design problems.

Acknowledgments H. Fan is partially supported by a graduate fellowship from Chinese Scholar Council (CSC), and this support is greatly appreciated.

References

Albert P, Schwarz U (2014) Dynamics of cell shape and forces on micropatterned substrates predicted by a cellular Potts model. Biophys J 106(11):2340–2352

Bischofs I, Schmidt S, Schwarz U (2009) Effect of adhesion geometry and rigidity on cellular force distributions. Phys Rev Lett 103(4):048101

Blake T (2006) The physics of moving wetting lines. J Colloid Interface Sci 299(1):1–13

Bostwick J, Shearer M, Daniels K (2014) Elastocapillary deformations on partially-wetting substrates: rival contact-line models. Soft Matter 10(37):7361–7369

Brill-Karniely Y, Nisenholz N, Rajendran K, Dang Q, Ramaswamy K, Zemel A (2014) Dynamics of cell area and force during spreading. Biophys J 107(12):L37–L40

Cai Y, Biais N, Giannone G, Tanase M, Jiang G, Hofman J, Wiggins C, Silberzan P, Buguin A, Ladoux B, Sheetz M (2006) Nonmuscle myosin IIA-dependent force inhibits cell spreading and drives F-actin flow. Biophys J 91:3907–3920

Chamaraux F, Fache S, Bruckert F, Fourcade B (2005) Kinetics of cell spreading. Phys Rev Lett 94(15):158102

Cuvelier D, Thery M, Chu Y, Dufour S, Thiery J, Bornens M, Nassoy P, Mahadevan L (2007) The universal dynamics of cell spreading. Curr Biol CB 17(8):694–699

Dobereiner H, Dubin-Thaler B, Giannone G, Xenias H, Sheetz M (2004) Dynamic phase transitions in cell spreading. Phys Rev Lett 93(10):108105

Douezan S, Guevorkian K, Naoua R, Dufour S, Cuvelier D, Brochard-Wyart F (2011) Spreading dynamics and wetting transition of cellular aggregates. Proc Natl Acad Sci USA 108(18):7315–7320

Dubin-Thaler B, Hofman J, Cai Y, Xenias H, Spielman I, Shneidman A, David L, Dobereiner H, Wiggins C, Sheetz M (2008) Quantification of cell edge velocities and traction forces reveals distinct motility modules during cell spreading. PLoS ONE 3(11):e3735

Edwards S, Yeomans J (2009) Spontaneous flow states in active nematics: a unified picture. EPL Europhys Lett 85(1):18008

Fardin M, Rossier O, Rangamani P, Avigan P, Gauthier N, Vonnegut W, Mathur A, Hone J, Iyengar R, Sheetz M (2010) Cell spreading as a hydrodynamic process. Soft Matter 6(19):4788

Frisch T, Thoumine O (2002) Predicting the kinetics of cell spreading. J Biomech 35(8):1137–1141

Gabella C, Bertseva E, Bottier C, Piacentini N, Bornert A, Jeney S, Forró L, Sbalzarini I, Meister J, Verkhovsky A (2014) Contact angle at the leading edge controls cell protrusion rate. Curr Biol CB 24(10):1126–1132

Giomi L, DeSimone A (2014) Spontaneous division and motility in active nematic droplets. Phys Rev Lett 112(14):147802

Gurtin E, Murdoch A (1977) Surface stress in solids. Int J Solids Struct 14:431–440

Hategan A, Law R, Kahn S, Discher D (2003) Adhesively-tensed cell membranes: lysis kinetics and atomic force microscopy probing. Biophys J 85(October):2746–2759

Hategan A, Sengupta K, Kahn S, Sackmann E, Discher D (2004) Topographical pattern dynamics in passive adhesion of cell membranes. Biophys J 87(5):3547–3560

Holzapfel G (2000) Nonlinear solid mechanics. Wiley, Chichester

Huang J, Peng X, Xiong C, Fang J (2011) Influence of substrate stiffness on cell-substrate interfacial adhesion and spreading: a mechano-chemical coupling model. J Colloid Interface Sci 355(2):503–508

Izrailev S, Stepaniants S, Isralewitz B, Kosztin D, Lu H, Molnar F, Wriggers W, Schulten K (1999) Steered molecular dynamics. In: Deuflhard P, Hermans J, Leimkuhler B, Mark A E, Reich S, Skeel R D (eds) Computational molecular dynamics: challenges, methods, ideas. Springer, Berlin, pp 39–65

Jagota A, Argento C (1997) An intersurface stress tensor. J Colloid Interface Sci 191(2):326–336

Joanny J, Prost J (2009) Active gels as a description of the actin-myosin cytoskeleton. HFSP J 3(2):94–104

Julicher F, Kruse K, Prost J, Joanny J (2007) Active behavior of the cytoskeleton. Phys Rep 449(1–3):3–28

Karcher H, Lammerding J, Huang H, Lee R, Kamm R, Kaazempur-Mofrad M (2003) A three-dimensional viscoelastic model for cell deformation with experimental verification. Biophys J 85(5):3336–3349

Kumar A, Maitra A, Sumit M, Ramaswamy S, Shivashankar G (2014) Actomyosin contractility rotates the cell nucleus. Sci Rep 4:3781

Li J, Han D, Zhao Y (2014) Kinetic behaviour of the cells touching substrate: the interfacial stiffness guides cell spreading. Sci Rep 4:3910

Lo C, Wang H, Dembo M, Wang Y (2000) Cell movement is guided by the rigidity of the substrate. Biophys J 79(1):144–152

McGrath J (2007) Cell spreading: the power to simplify. Curr Biol 17(10):R357–R358

Minaki H, Li S (2014) Multiscale modeling and simulation of dynamic wetting. Comput Methods Appl Mech Eng 273:273–302

Nisenholz N, Rajendran K, Dang Q, Chen H, Kemkemer R, Krishnan R, Zemel A (2014) Active mechanics and dynamics of cell spreading on elastic substrates. Soft matter 10(37):7234–7246

Ofer N, Mogilner A, Keren K (2011) Actin disassembly clock determines shape and speed of lamellipodial fragments. Proc Natl Acad Sci USA 108(51):20394–20399

Roy S, Qi H (2010) A computational biomimetic study of cell crawling. Biomech Model Mechanobiol 9(5):573–581

Sackmann E, Bruinsma R (2002) Cell adhesion as wetting transition? Chemphyschem Eur J Chem Phys Phys Chem 3(3):262–269

Sauer R (2006) An atomic interaction based continuum model for computational multiscale contact mechanics by. Dissertation, University of California, Berkeley

Sauer R, Li S (2007a) A contact mechanics model for quasi-continua. Int J Numer Methods Eng 71:931–962

Sauer R, Li S (2007b) An atomic interaction-based continuum model for adhesive contact mechanics. Finite Elements Anal Des 43(5):384–396

Sauer R, Li S (2008) An atomistically enriched continuum model for nanoscale contact mechanics and its application to contact scaling. J Nanosci Nanotechnol 8(7):3757–3773

Shikhmurzaev YD (2006) Singularities at the moving contact line. Mathematical, physical and computational aspects. Phys D Nonlinear Phenom 217(2):121–133

Style R, Che Y, Park S, Weon B, Je J, Hyland C, German G, Power M, Wilen L, Wettlaufer J, Dufresne E (2013) Patterning droplets with durotaxis. Proc Natl Acad Sci USA 110(31):12541–12544

Sun L, Cheng Q, Gao H, Zhang Y (2009) Computational modeling for cell spreading on a substrate mediated by specific interactions, long-range recruiting interactions, and diffusion of binders. Phys Rev E 79(6):061907

Vernerey F, Farsad M (2011a) A constrained mixture approach to mechano-sensing and force generation in contractile cells. J Mech Behav Biomed Mater 4:1683–1699

Vernerey F, Farsad M (2011b) An Eulerian/XFEM formulation for the large deformation of cortical cell membrane. Comput Methods Biomech Biomed Eng 14:433–445

Vernerey F, Farsad M (2014) A mathematical model of the coupled mechanisms of cell adhesion, contraction and spreading. J Math Biol 68(4):989–1022

Viamontes J, Narayanan S, Sandy AR, Tang JX (2006) Orientational order parameter of the nematic liquid crystalline phase of F-actin. Phys Rev E, 73(6):061901

Viamontes J, Tang JX (2003) Continuous isotropic-nematic liquid crystalline transition of f-actin solutions. Phys Rev E, 67, article no. 040701

Vianay B, Kafer J, Planus E, Block M, Graner F, Guillou H (2010) Single cells spreading on a protein lattice adopt an energy minimizing shape. Phys Rev Lett 105(12):128101

Wakatsuki T (2003) Mechanics of cell spreading: role of myosin II. J Cell Sci 116(8):1617–1625

Wilson C, Tsuchida M, Allen G, Barnhart E, Applegate K, Yam P, Ji L, Keren K, Danuser G, Theriot J (2010) Myosin II contributes to cell-scale actin network treadmilling through network disassembly. Nature 465(7296):373–377

Wolfenson H, Iskratsch T, Sheetz M (2014) Early events in cell spreading as a model for quantitative analysis of biomechanical events. Biophys J 107(11):2508–2514

Young T (1805) An essay on the cohesion of fluids. Philos Trans R Soc Lond 95:65–87

Zemel A, Rehfeldt F, Brown AEX, Discher DE, Safran SA (2010) Cell shapes, spreading symmetry, and the polarization of stress-fibers in cells. J Phys: Condens Mat 22(19):194110

Zeng X, Li S (2011a) Modelling and simulation of substrate elasticity sensing in stem cells. Comput Methods Biomech Biomed Eng 14(5):447–458

Zeng X, Li S (2011b) Multiscale modeling and simulation of soft adhesion and contact of stem cells. J Mech Behav Biomed Mater 4(2):180–189

Zeng X, Li S (2012) A three dimensional soft matter cell model for mechanotransduction. Soft Matter 8(21):5765